COMPUTATIONAL AERODYNAMIC ANALYSIS ON A GENERIC UCAV/URAV CONFIGURATION

Yngve C-J Sedin, Ingemar Persson, Henrik Åslund
Saab Aerosystems
Flight Physics - Aerodynamics and Flight Mechanics
SE-58188 Linköping

Keywords: *Aerodynamic analysis, computational aerodynamics, configuration, UCAV, URAV*

Abstract

A short study was carried out on a generic multi-role utility UCAV/URAV (Unmanned Combat/Reconnaissance Aerial Vehicle) configuration. Specifications called for high speed at low altitude and a combined utility as long range reconnaissance at medium altitude. Payloads are kept inside the fuselage. The configuration was a swept wing-fuselage combination having an aft V-tail and an upper fuselage air intake with a rear jet nozzle. The fore-body shape provoked vortex flow separation. Vortex flow was influencing on stability. The aft V-tail was exposed in this flow.

Baseline design and derivatives were mainly analyzed using in-viscid Euler with sparse checks using a Navier-Stokes flow solver, all applied to unstructured grids. Calculations showed fore body vortex flow and separation on outboard wing parts affecting stability. Re-design of the wing relieved outer wing load giving improvements. Longitudinal stability is analyzed and different methods are compared.

1 Introduction

The cost spiral of development of military equipment is a strong driver for finding new and more cost effective solutions breaking the upward trend. Hence there is a need for seeking compromised multi utility concepts achieving cost effectiveness but still with good performance in all roles using new technology. Requirements about good performance and reasonably good flying handling qualities based on proven experience sometimes lead to conflicting design when matched against tactics driven by new enabled technology. One example is the obvious conflict between aerodynamic shaping for good performance, stability and control, versus geometric requirements coming from low radar signature for stealth properties. Functional compromises are then needed. This is also true for staying inside optimized cost frames.

During the last 10-15 years, Unmanned Aerial Vehicles (UAV) have attracted increased interest for many obvious reasons. In early 2005, a short generic investigation, of which Ref [10] is but one part, was initiated and supported by the Swedish Air Material Defense Agency (FMV) to study a combined mission utility UCAV/URAV concept. A reasonably compromised configuration was compared with that of a more extreme blended configuration, thus emphasizing very low Radar Cross Signature (RCS) such as the diamond shaped Saab FILUR vehicle. This paper presents aerodynamic analysis on the compromised configuration and constitutes one sub part of the report in Ref [10].

This generic study ended up in a 12t class configuration having a wing span of the order of 13m with 2t internally kept payload and a range of up to about 800NM. The configuration consisted of a swept wing fitted to a fuselage with an aft V-tail. It was designed for transonic speed at low to medium altitudes emphasizing good transport economy.

This paper briefly gives some background of the outlined configuration showing computational results of the aerodynamic analysis. The intention was to proceed with wind tunnel testing but this was not pursued.

2 General

2.1 Multi-role philosophy

During the 70's, national procurement studies were ongoing in Sweden for a successor to the Saab 37 Viggen (Fig 1) fighter in attack role.

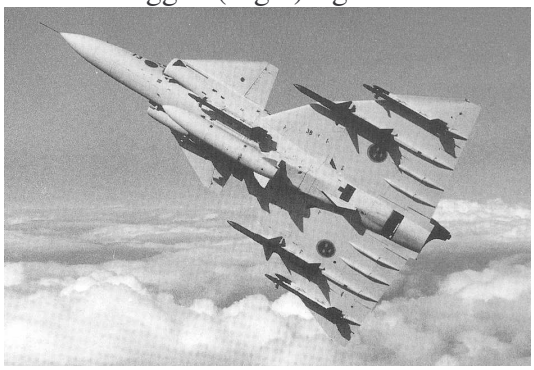

Fig 1. Saab 37 Viggen.

The specification called for subsonic low level missions flown well into transonic. Much of the research work was focused on low transonic drag with implications on e.g. the choice of wing airfoils and area distributions some experiments reported in Ref [1]. This emanated in a configuration called B3LA, represented by the wind tunnel (W/T) model shown in Fig 2.

Fig 2. B3LA wind tunnel (W/T) model.

In 1979 the B3LA program was cancelled. Instead a new decision was taken to go ahead with a true multipurpose supersonic swing role fighter taking on all missions, ground attack, interceptor and reconnaissance in one design having an onboard airborne swing role capability. With this, cost effectiveness would be achieved and the trend for ever increasing cost and aircraft size should be broken. The first years of intensive development led to the Saab 39 Gripen layout, as seen in Fig 3.

Fig 3. Saab 39 Gripen, the 1st operational 4th generation multi-role fighter.

Although the Gripen predecessor, Saab 37 Viggen, bore the idea of being a united triple multi-role concept, they were all mainly developed and operated in different versions for ground attack, interceptor and reconnaissance.

In the present generic UCAV/URAV study, the traditional idea of a single platform being able to operate in two roles was pursued much in line with previous philosophy for Saab 39 Gripen and the Saab 37 Viggen. Moreover, for reasonable compromises around transport economy, stealth requirements and low altitude high speed penetration, a swept wing- aft tail configuration, Fig 6, was chosen for the various demands, ranging from both UCAV to URAV.

Experience from swept wing aft tail designs were reused where possible. This embodied B3LA (Fig 2) and in some respect even back to the 50's and Saab 32 Lansen, Fig 4, and the 60's through the trainer Saab 105.

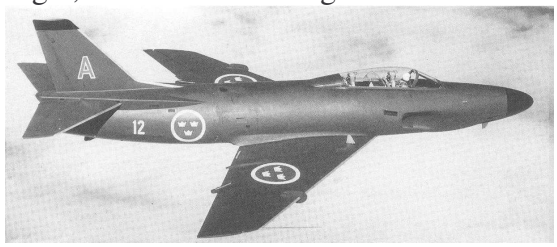

Fig 4. Saab 32 Lansen.

Traditional tactical multi-operational ideas were adopted, but now with requirements about stealth properties, fairly long range and with internally stored payload in challenging focus.

2.2 Recycled Technology

During the 70's much aerodynamic research was devoted to high-speed supercritical wing design and a renewed interest in the transonic equivalence rule, see e.g. Refs [1]-[5]. This was spurred by the interest in transonic and supersonic flight and the ongoing rapid development in numerical computation. In preparation for the B3LA development (Fig 2), this was ongoing at Saab and FFA (now FOI). As one result a wing (Fig 5) was wind tunnel tested at FFA and late reported in Ref [1].

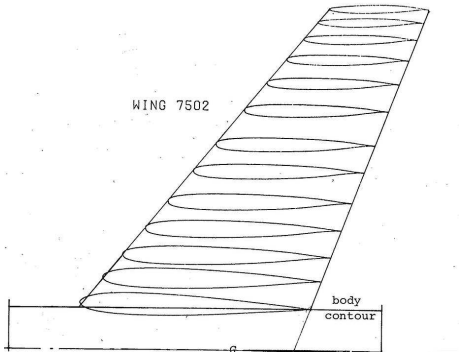

Fig 5. Research Wing 7502

In the present UCAV/URAV study the same research wing (Fig 5) was rescaled to fit the new application, see the generic UCAV/URAV configuration in Figs 6-7. After preliminary analysis, changes to the wing leading edge as well as wing twist and taper ratio were called for improving the baseline design at high angles of attack (AoA). The Wing 7502 was designed for high-speed transonic at low lift coefficients that did not entirely suit requirements at moderate Mach numbers and higher lift coefficients. An upper side nose suction pressure peak was terminated with a forward shock wave. Design changes were accordingly taken for improvements.

2.3 UCAV/URAV Configuration

Specifications and operational requirements led to a configuration having a swept wing and an aft V-tail all mounted to a characteristic fairly flat fuselage with an upper air intake as shown in Figs 6-7. Reasonable compromises were made balancing radar signatures and aerodynamic shaping for transport economy with manageable stability and control. However, there are latent aerodynamic problems with an aft V-tail exposed in local vortex flow partly coming from wedge like longitudinal fore body side edges of the stealth shaped fuselage at high angles of attack.

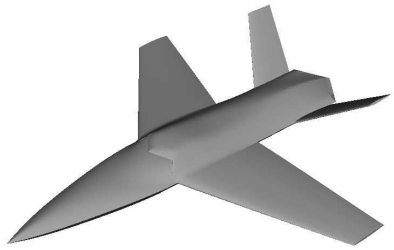

Fig 6. UCAV/URAV configuration, 2510.

Overall cross section area distribution having implications on transonic drag-rise is depicted in Fig 7.

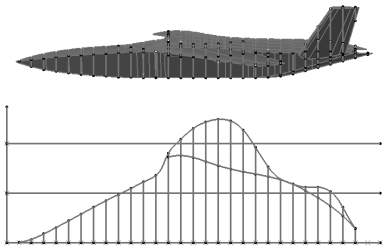

Fig 7. Cross section area distribution, 2510.

Incoming and outgoing stream tubes are not shown, Fig 7. For area-rule considerations, inlet and outlet must be added at defined drag and engine reference conditions, Ref [4].

The final wing had a leading edge sweep of around 34°, aspect ratio 4.6 and taper ratio 0.33. Wing thickness ranged from inboard 9.6% to outboard 8.2% and the non-linear wing twist was about -5° from root to tip, see Fig 12.

2.4 Computational Approach and Methods

Considering the effective three month short engineering effort on the project (Ref [10]), most analysis were carried out using in-viscid computational methods. The national 3D

computational fluid dynamics (CFD) code EDGE, see Ref [6], was run mainly in Euler mode with sparse checks run in Navier-Stokes mode. Rapid estimations of aerodynamic derivatives for comparison were performed using a linear panel method similar to Ref [7]. Limited 2D analysis for qualitative guidance of local geometry changes of airfoil sections was performed using the Euler streamline curvature method, MSES Ref [8], with surface boundary layer of classic integral type. 2D local geometry changes in the nose region were carried out by 'PROFAN', Ref [9], by working on split coordinates in terms of camber and thickness and then recombining them. 3D lofting was carried out in CATIA V4 with information to the unstructured grid generation.

3D grid generation was performed using the hybrid (tetrahedral/prismatic) ICEM CFD V5.1 software. All flow calculations were parallelized and executed on in-house PC clusters. The number of grid nodes in Euler mode was about 1.5-3.2 million. Execution wall clock time was of order 5-15 hrs, depending on Mach number and angle of attack, when executed on 8-10 processors using 3 levels of multi-grid cycles. In Navier-Stokes mode the number of grid nodes was about 18 million working on 32 processors. Cell volumes close to wall surfaces were strived for to have a size equal to the classic y^+ measure normal to the wall in areas for high wall resolution. Turbulent flow was assumed all over and the Wallin-Johansson Ref [11] EARSM turbulence model with Hellsten Ref [12] wall model was applied. One computed case in viscous mode took about 100 wall clock hours depending on Mach number and angle of attack.

3 Development Strategy and Preliminaries

3.1 Line of Strategy

The main features of the UCAV/URAV configuration were first conceptually outlined. This was to broadly match requirements of performance specifications including payload, stowing of equipment and systems and principles of load carrying structures. Reasonable compromises were settled and stealth properties and other considerations were taken into account. Baseline design came out similar to the configuration presented in Fig 6.

A number of evolutionary steps were then taken to check aerodynamics, stability and control as well as improving on sizing and shaping. The steps are shown in Table 1 below

Table 1. Computational development history.

Conf ID	Components	Γ_T^o	θ_W^o	Remark
2505	W	-	-2.3	Scaled W7502
2507	W	-	-2.8	Twist added
2507*	W+B+T	50	-2.8	Dressed up
2508-1	W+B+T	50	-3.8	Twist added
2508-2	W+B+T	45	-3.8	Modified Tail
2508-2	W+B	-	-3.8	Tail off
2508-3	W+B	-	-3.8	Modif. W+B
2508-4	W+B+T	-	-3.8	Modified W
2508-6	W+B	-	-5.1	Twist added
2509-1	W+B	-	-5.1	Modified B
2509-1*	W+B+T	45	-5.1	Dressed up
2510	W+B+T	40	-5.1	Final, mod B
2510-1[1]	W+B+T	-5.0	-5.1	Final, mod T

Notations: W wing, B fuselage, T tail, Γ_T^o tail dihedral, θ_W^o is total wing twist from root to tip. (.)* Distinguish same configuration ID, but fully dressed. (.)[1] Special investigation for no tail dihedral, Γ_T^o=-5.0.

Evolution development going from 2508-3 down to 2509-1 (Table 1) can be seen in Fig 8.

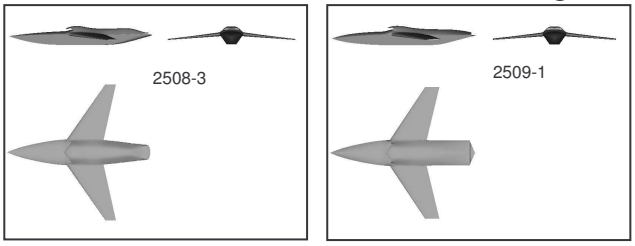

Fig8. Configuration changes (W/B), ref Table1.

Starting with the wing only geometry named 2505, derived from wing W7502, Fig 5; thirteen

different configurations (Table 1) were leapt through ending up with the final 2510 and the separate tail investigation, 2510-1. For the third last, 2509-1*, both longitudinal and lateral stability were computed as well as drag from Mach 0.2 up to Mach 0.85. The present paper will limit to longitudinal stability and drag. The final 2510, with local changes to the aft jet outlet and the air intake compared to 2509-1*, will be presented including sparse comparisons between viscid and in-viscid calculations.

3.2 Initial Calculations

Main features and behavior of wing only and full configuration were initially investigated by leaping through the first three; 2505, 2507 and 2507* , see Table 1. During this the wing twist was increased by half a degree to -2.8°. Analyzing the fully dressed up 'baseline' design 2507*, regarding the local lift distribution Fig 9; it was revealed that separation occurred on outboard wing with increasing angle of attack.

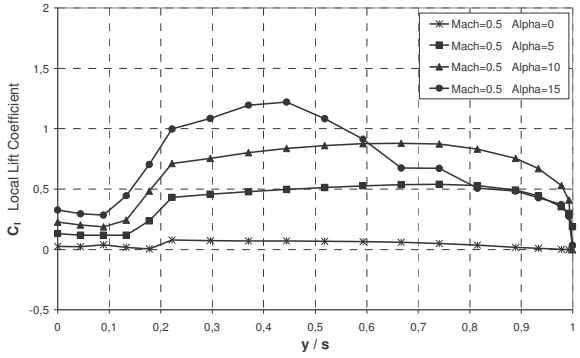

Fig 9. Spanwise wing lift coefficient distribution of 'baseline' design 2507* at Mach 0.5.

The local lift coefficient reached its maximum at about 70% of half the wing span. At angle of attack α=15°, the outboard wing became separated and stalled. To improve on this, a number of actions were taken going all the way from 2507* to 2508-4 in Table 1. One way was to increase the wing twist; another was to increase the wing taper ratio and slightly reducing the span keeping the wing area. Moreover, moderate local wing leading edge changes were made by adding camber line nose droop and at the same time slightly reducing the symmetric leading edge nose thickness by operating the PROFAN geometry manipulation method, Ref [9]. Leading edge modifications are shown in Fig 10 for the wing airfoil in the section located at 2/3 of half the wing span.

Qualitative 2D MSES Ref[8] calculations on original and modified airfoils (Fig 10) at Mach 0.5 indicated about 20% reduction in the nose upper surface pressure suction peak at 5° angle of attack. An isentropic re-compression was obtained with no appearing forward shockwave at Mach 0.5. Checks in transonic showed no decisive aerodynamic degradation inside the operational envelope up to Mach 0.85 because of made modifications. This type of nose, Fig 10 modification, was then for simplicity applied all over the wing, 4° additional nose droop and a nose thickness reduction factor 0.8.

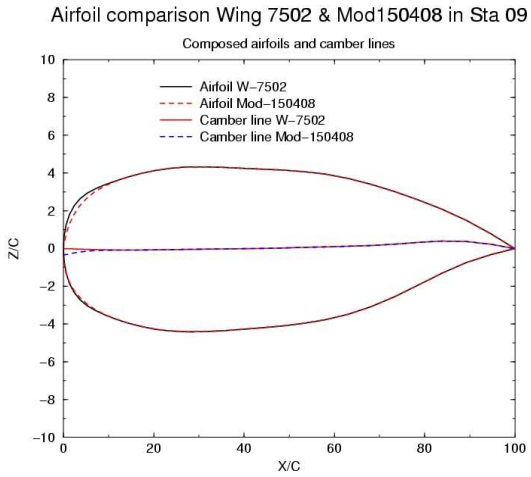

Fig 10. Wing leading edge modification.

Leading edge changes were applied ahead of 15% wing chord. Continuity was ensured in all derivates up to second order at the attachment.

With mentioned modifications leaping all the way from 'baseline' design 2507* up to 2508-4, the latter showed improvements, Fig 11, and no tendency for an early outboard wing separation at α =15° at the lower Mach 0.2. Wing twist distributions going from base line 2507* to the final introduced in 2508-6 can be seen in Fig 12. More twist is not recommended due to additional drag at high speed flight.

Although the analysis around Fig 9 was based on in-viscid Euler calculations it is thought this still has qualitative relevance as the momentum equation is fulfilled. The real test will come with the Navier-Stokes flow solver. However, one is confronted by uncertainties in

physical modeling of turbulence in separated flows and lack of interactive simulation of laminar-turbulent transition mechanisms.

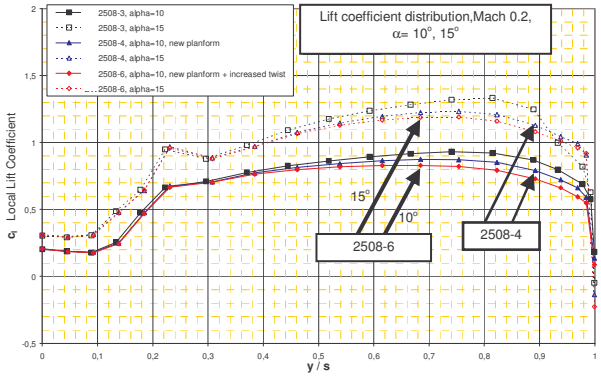

Fig 11. Wing lift coefficient distribution of 2508 development at Mach 0.2 and α=10°, 15°.

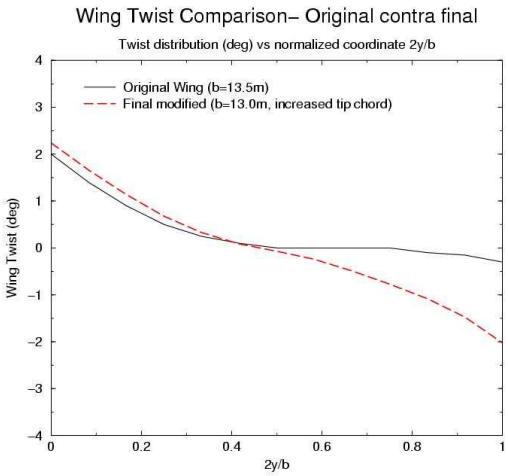

Fig 12. Wing twists distributions.

3.3 Linear Theory Aerodynamic Derivatives

For comparison with non-linear methods, linear theory panel method calculations were performed yielding qualitative derivatives for the last two configurations in Table 1 (2509-1 and 2510). The panel model having 2x399 panels can be seen in Fig 13. Longitudinal stability results are shown in Table 2.

Table 2 indicates there is room for shifting center of gravity (CG) backward or possibly the wing and tail set somewhat forward for a better balanced, less statically stable configuration.

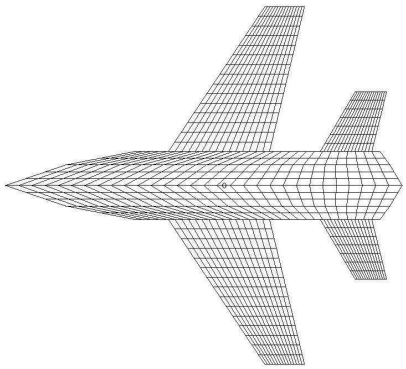

Fig 13. Panel model of 2509-1* and 2510.

Table 2. Longitudinal stability derivatives, linear theory. Configurations 2509-1* and 2510.

Mach	$C_{N\alpha}$	$C_{m\alpha}$	$X_{NP}=C_{m\alpha} / C_{N\alpha}$
0.2	4.8270	-0.6924	-0.1434
0.5	5.0995	-0.7762	-0.1522
0.8	5.8477	-1.0116	-0.1730
0.85	6.0840	-1.0867	-0.1786

Notation: C_N, normal force; C_m, pitching moment. Static margin $X_{NP}<0$ for stability.

4 Results

4.1 Aerodynamics of Configuration 2509-1*

Figs 14-19 show aerodynamic characteristics computed by EDGE in Euler mode. Table 3 shows a comparison between the non-linear Euler and the linear panel method concerning derivatives and stability margins in the vicinity of zero angle of attack.

Looking at the normal force $C_N(\alpha)$, Fig 14, the Mach 0.5 is clearly standing out compared to all computed Mach and shows fairly sudden

losses of C_N starting more severely at $\alpha=12^o$. This is confirmed by the break away and loss of in-plane wing suction forces illustrated by the tangential force $C_T(\alpha)$ in Fig 17.

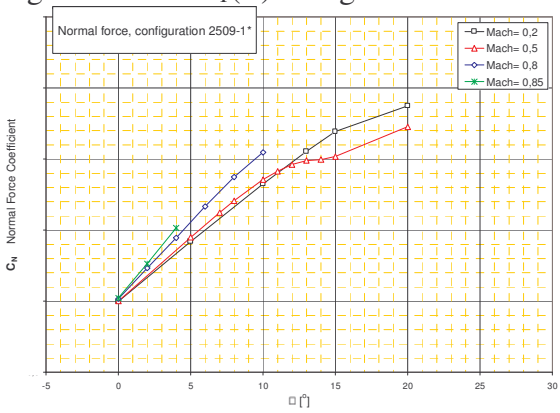

Fig 14. Normal force $C_N(\alpha;Mach)$, 2509-1*.

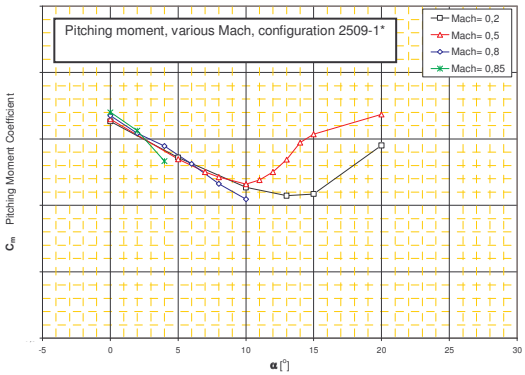

Fig 15. Pitching moment $C_m(\alpha;Mach)$, 2509-1*.

The classic swept wing pitch-up takes on even earlier at about $\alpha=10^o$, see $C_m(\alpha)$ in Fig 15. The reason for all this was found in flow field observations in terms of streamlines and pressures mapped on the wing surface, see Fig 18, but also due to an apparent destabilizing effect by the tail exposed in combined nonlinear downwash from the wing and the strong fore body vortices, see C_m in Fig 16 and tail off cross-flow in Fig 19. Fig 18 shows the beginning of an outboard wing separation that gradually spreads with α leading to losses of lift behind the pitch reference axis.

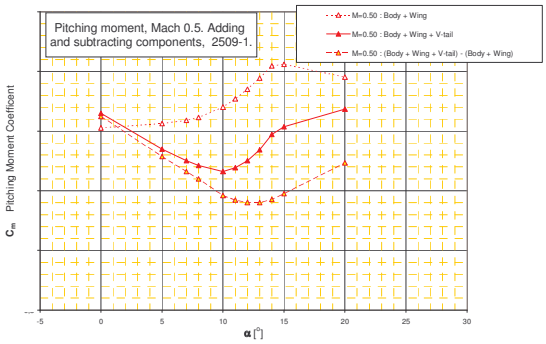

Fig 16. Pitching moment $C_m(\alpha)$. Stripping off components deriving tail contribution at Mach 0.5, 2509-1*.

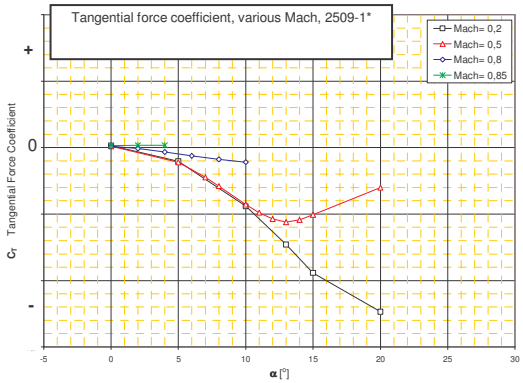

Fig 17. Tangential force $C_T(\alpha;Mach)$, 2509-1*.

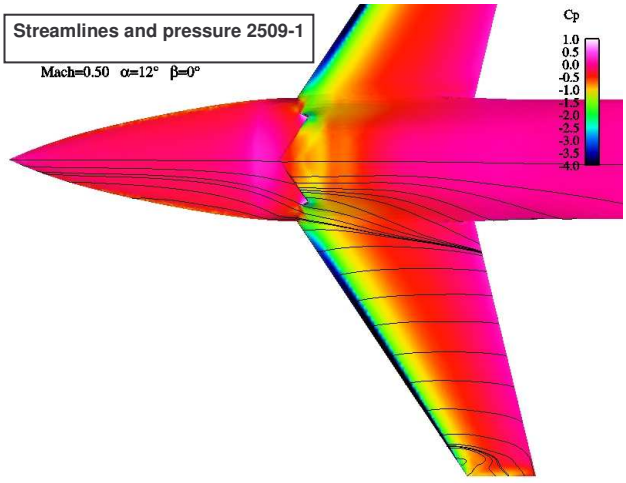

Fig 18. Beginning of outboard wing separation at $\alpha=12^o$, Mach = 0.5. In-viscid results of 2509-1.

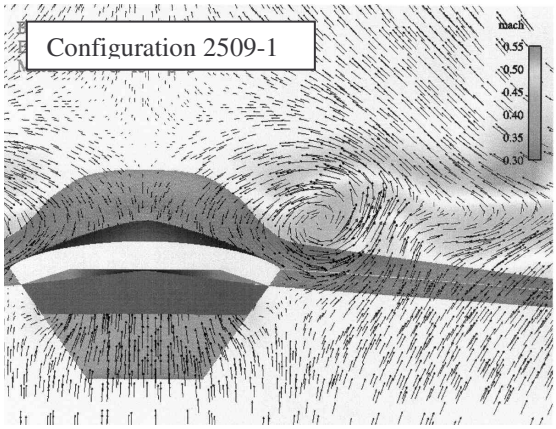

Fig 19. Tail-off cross-flow velocity in plane at tail position. Mach 0.5, $\alpha=15^o$.

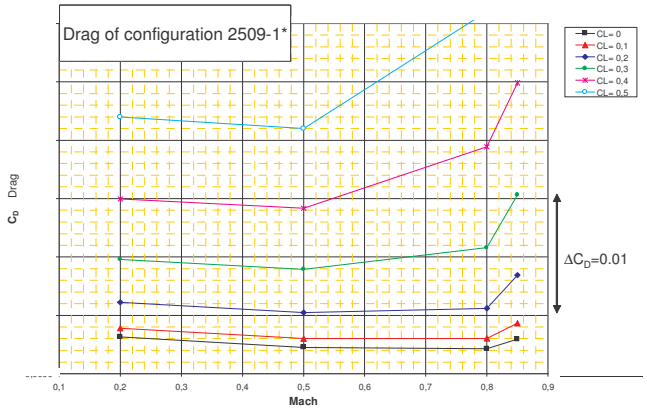

Fig 20. Drag force C_D(Mach;C_L), 2509-1*.

It is evident that design counters measures taken in the wing leading edge area, including twist and increased taper ratio, was not enough. They could not postpone α for pitch-up further than to about $\alpha=12^o$ at Mach 0.5, evaluations so far done only in-viscidly. More work is needed to the outboard wing avoiding upper shock induced separation at intermediate flight Mach. At low speed and in transonic, the situation is better, a fact that was also noted in the wind tunnel tests in Ref [1].

Turning the attention to the drag C_D, this was computed in Euler mode for 2509-1* and is shown in Fig 20 as function of Mach with the lift coefficient C_L as a parameter. Apparently the zero lift drag-rise Mach number, found at gradient $dC_D/dM=0.1$ (M is Mach number), is well above Mach 0.85. Objectives were then met for high speed low level missions at low lift coefficients. A qualitative evaluation of an Oswald efficiency factor for lift induced drag gave an e-value around 0.92 that is reasonably good, but still evaluated in an in-viscid analysis.

In Table 3, a relative comparison in the vicinity of AoA $\alpha=0^o$ is shown between linear panel method results and computed nonlinear Euler data regarding longitudinal stability derivatives. All variables are taken with their proper signs and differences are all normalized by linear data from Table 2. From Table 3 one can see that linear theory in comparison with nonlinear gradually under predicts the normal force slope for increasing Mach and at Mach 0.85 it is about 13%. On the other hand the static stability is over predicted using linear theory. With nonlinear theory, in relative terms compared to linear, the pitching moment slope is gradually reduced towards the positive side. At Mach 0.2 the reduction is about 7% and at Mach 0.85 it is as much as 30%.

This is all reflected in the normalized neutral point (NP) location X_{NP}, see Table 2 and Table 3. X_{NP} is here equivalent to the static margin referenced to the pitch axis. By NP definition in Table 3 one can conclude that this point is moved forward using nonlinear theory compared to linear. It moves in closer to the reference pitch axis with about 6.7% at Mach 0.2 and as much as 35.9% at Mach 0.85.

Table 3. Comparison of stability derivatives, nonlinear contra linear theory, 2509-1* at $\alpha=0$: 100[(Nonlinear x_α)-(Linear_x_α)]/(Linear_x_α).

Mach	$\%\Delta C_{N\alpha}/C_{N\alpha}$	$\%\Delta C_{m\alpha}/C_{m\alpha}$	$\%\Delta X_{NP}/X_{NP}$
0.20	-0.3	-7.0	-6.7
0.50	+1.1	-12.7	-13.6
0.80	+5.4	-25.9	-29.7
0.85	+13.0	-30.0	-35.9

Note: $X_{NP}=C_{m\alpha}/C_{N\alpha}$. For static stability is $X_{NP}<0$ and the neutral point (NP) located behind the ref axis.

These differences between linear and nonlinear theory constitute the nonlinear higher fidelity modeling of physics and mathematics. At intermediate Mach numbers down to low, the agreement between the theories is surprisingly

good, although the panel model is just built by planar lifting surfaces as shown in Fig 13.

4.2 Aerodynamics of Configuration 2510

Some geometric modifications were made locally to configuration 2509* around the air intake and at the jet nozzle outlet. This version, called 2510 in Table 1, became the final as far as the present study proceeded. When differences between 2509* and 2510 were considered to be small for overall aerodynamic characteristics, the subsequent analysis on 2510 was limited to aerodynamics at Mach 0.5.

A special investigation of tail efficiency was initiated, related to the vortex wake from the fore body and the wing (see in Fig 16 and Fig 19). This was done by setting the tail dihedral angle to -5° for 2510-1, see Table 1. The effect on static stability by pivoting the tail away down under the wake can be seen in Fig 21. 2510-1 with -5° dihedral is compared in Fig 21 with 2510 and 2509* having 40° and 45° tail dihedral (Table 1).

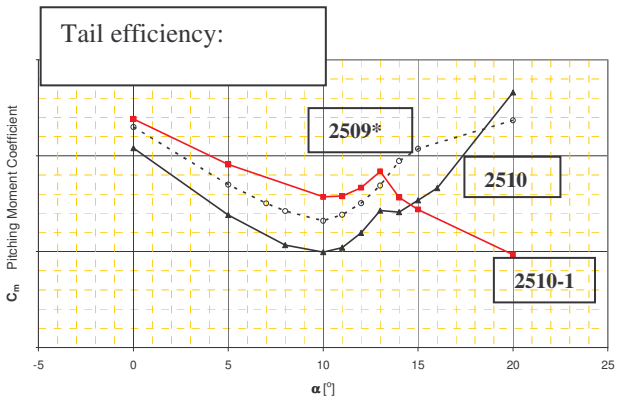

Fig 21. Effect of tail dihedral on in-viscid pitching moment $C_m(\alpha)$ at Mach 0.5. 2510 and 2509* compared to 2510-1 with -5° dihedral.

A drastic stability improvement for 2510-1 is demonstrated in Fig 21 compared to 2510 and 2509*. However, a pitch up is found between α=11-13°. This is still likely due to separation on outboard wing part behind the pitch reference axis. This could be improved by reducing the outer wing load through an increased wing tip chord and further re-design of the leading edge. However, with reduced or no tail dihedral, the directional lateral stability will be lost calling for other aerodynamic means or vectored thrust regaining lateral stability and control without degrading stealth properties. It could be a vertical fin or better a set of V-fins, like the Saab Sharc UAV test vehicle, but longitudinally staggered ahead of the horizontal stabilizer having little or no dihedral. This is the natural place for filling out and smoothing the area distribution, important at transonic speed, see cross-sectional area distribution in Fig 7.

Finally viscous analysis using the Navier-Stokes (N-S) solver in Ref [6] applied to 2510 (Table 1) will be presented, see Figs 22-24.

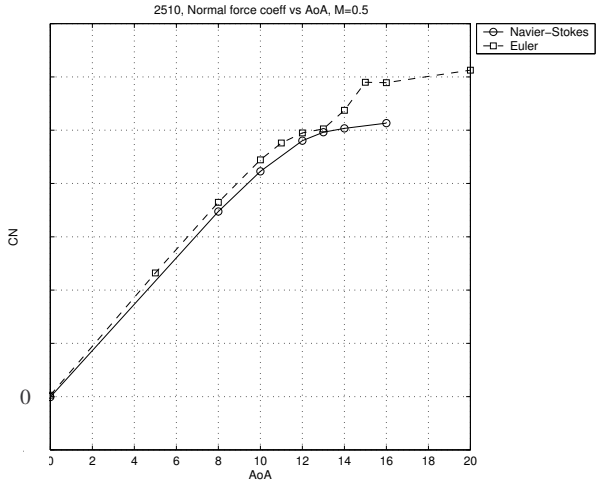

Fig 22. Normal force $C_N(\alpha)$ of 2510 at Mach 0.5, viscid N-S and in-viscid Euler calculations.

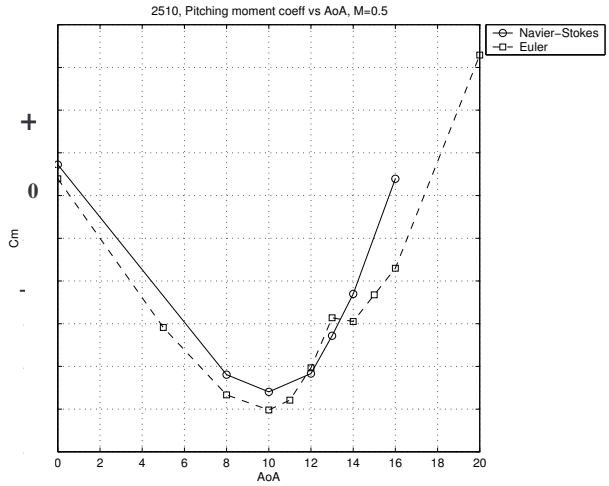

Fig 23. Pitching moment $C_m(\alpha)$ of 2510 at Mach 0.5, viscid N-S and in-viscid Euler calculations.

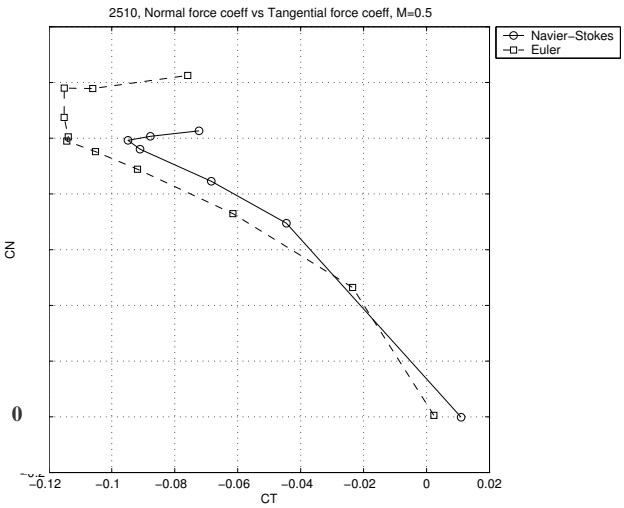

Fig 24. In-plane suction force C_T plotted via normal force C_N of configuration 2510 at Mach 0.5, a comparison of viscid and in-viscid results.

Looking at Fig 22, the viscous Navier-Stokes solution seems to smooth out local obstructions likely coming from differences in the substructure of occurring flow separations. The N-S solution is smoothing out details of in-viscid behavior. The latter sometimes showing up fluctuations in the solution like un-damped limit cycle oscillations at high AoA.

By large, the N-S pitching moment characteristics, Fig 23, typically maintain the trend experienced in the Euler results. The N-S results are also smoother than the corresponding Euler data. The static stability for small AoA is slightly reduced in the viscid solution. The classic disease of swept wing outboard separation, contributing to pitch up, is still there as well as the vortex interference and downwash on the V-tail.

Finally, Fig 24 is showing the break down of in-plane tangential wing suction forces, C_T, with increasing C_N. Even here viscosity is slightly changing the behavior and the breakdown now comes surprisingly sudden and abrupt compared to the Euler solution. Qualitatively extracting lift dependent drag, in connection with N-S computed (C_N,C_T), an Oswald efficiency factor of about e=0.82-0.90 depending on the lift coefficient (C_L=0.5-->0.3) came out. This is an efficiency reduction compared to previous in-viscid Euler data of 2509-1* that indicated an

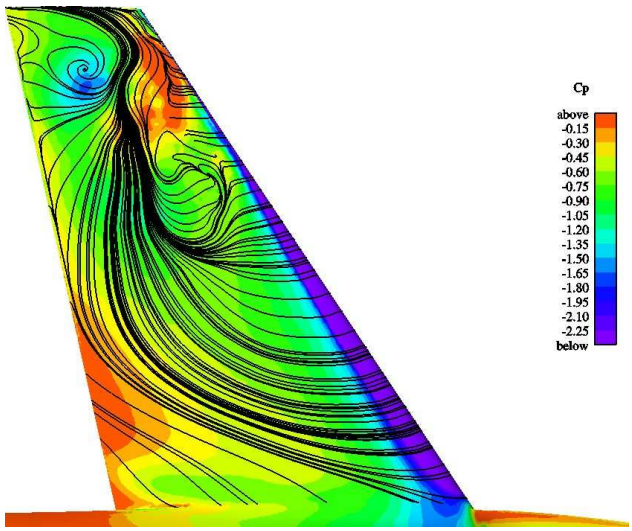

Fig 25. Pressure Cp and wing upper surface streamlines, Euler calculations on 2510 at Mach 0.5 and α=14°.

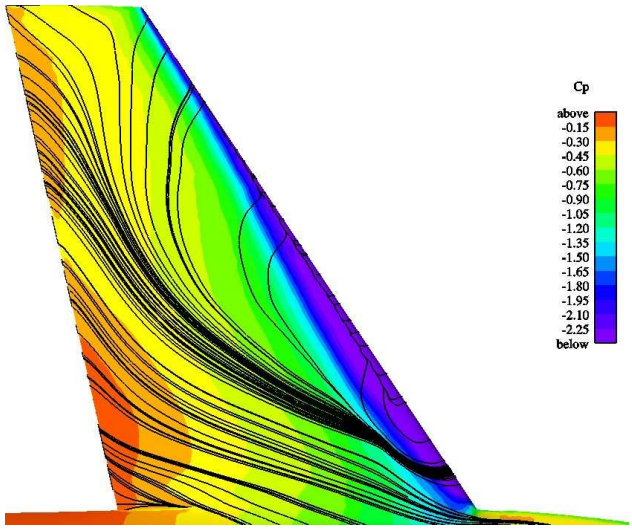

Fig 26. Pressure Cp and wing upper surface streamlines in wall boundary layer (approx y^+=10), Navier-Stokes calculations on 2510 at Mach 0.5 and α=14°.

e-value of about 0.92 in the same range of C_L-operation.

Figs 25-26 show non-dimensional wing upper surface pressures C_p and streamlines of the full configuration 2510. Fig 25 presents in-viscid Euler data while Fig 26 shows Navier-Stokes computed pressure and streamlines. Data are exposed at Mach 0.5 and α=14°.

In Fig 25 distinct outboard wing flow separations are recognized with converging streamlines and two separate rose patterns. One

of them has a clean spiral type vortex pattern, lifting and transporting flow off from the surface. In this case the overlaid pressure map is reflecting the streamlines fairly well when the flow is in-viscid. In Fig 26, however, the flow does not seem to have such clear features, but shows strong span-wise transport of boundary layer material and a bundle of densely packed streamlines, slowly diverging in the local flow direction. The flow interpretation is not so clear and easy to make here as the streamlines are traced inside the boundary layer. However, the surface pressure is more smoothly smeared out. Viscous terms in the N-S equations do produce solutions smearing kinks and wiggles in integrated forces and moments shown in the in-viscid Euler results presented earlier in Figs 21-23. Inherent in-viscid nonlinear flow instabilities in the Euler equations are naturally damped by shear stresses due to viscosity in Navier-Stokes equations. Results are then more smeared out and gradually developed with angle of attack as shown in the integrated forces and moments.

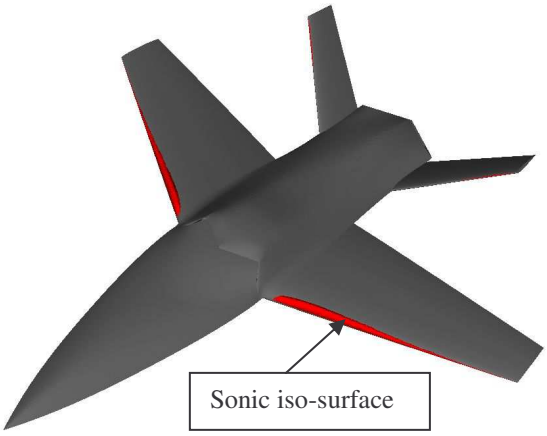

Fig 27. Sonic iso-surface at upper wing leading edge of conf. 2510 at flight Mach 0.5 and α=14^o. Flow computed by Navier-Stokes solver.

From Fig 27 it is obvious that a local supersonic region is created along the wing leading edge at angle of attack 14^o and flight Mach 0.5 even in viscid N-S flow solutions. The downstream termination of the sonic surface indicates the shock location. Apparently, measures taken for geometric improvements were not enough to prevent the 3D leading edge wing flow to go supersonic. The local inflow angle towards the inboard leading edge is geared up in front of the wing by the fuselage cross flow set up by the width of the body plus the fore body nonlinear vortex flow separation. A closer look at the V-tail reveals the same type of phenomena degrading the efficiency of the tail. Hence even the tail should be provided with a non symmetric airfoil to improve efficiency.

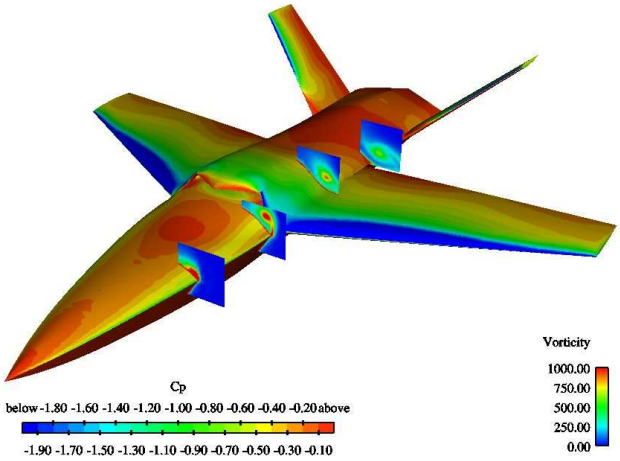

Fig 28. Surface pressure C_p and fore body separated vorticity mapped on local cross-flow planes. Configuration 2510 at Mach 0.5 and angle of attack α=14^o.

The figure above is illustrating surface pressure distributions Cp, corresponding with the sonic iso-surface condition in Fig 27 of configuration 2510. In addition local vorticity as separated from the fore body side edges of the fuselage is also shown in cross-flow planes. The flight Mach is 0.5 and the angle of attack is α=14^o.

5 Concluding remarks

A generic dual role UCAV/URAV configuration was studied. Overall design considerations led to a compromised layout balancing flight performance and stealth properties. The outcome was a swept wing

fuselage combination with an aft V-tail. Performance requirements were generally met with low altitude high speed flight in transonic and a reconnaissance role at intermediate altitude, all with reasonably good transport economy. Basic aerodynamic characteristics were satisfactorily met, but work on control aerodynamics largely remains.

Longitudinal stability and drag were presented as well as a short outlook on tail efficiency. Aerodynamic analysis was carried out using in-viscid Euler calculations with some sparse checks at intermediate speed using Navier-Stokes computations. Methodological comparisons between linear and nonlinear theory were assessed. Surprisingly good agreement regarding stability was obtained at low to intermediate Mach at small angles of attack.

Nonlinear analysis revealed separated fore body vortex flow passing downstream interacting with the tail plane. At high angles of attack, the V-tail could not counteract fore body lift increase and losses of wing lift due to outboard wing separation rendering pitch up tendencies. Re-design measures comprised increased negative wing twist and an increased wing taper ratio relieving outer wing load. Wing leading edge changes were made by camber nose droop and reducing nose bluntness. All changes were made in front of 15 % wing chord. The idea was to avoid forward shock induced wing separation at intermediate Mach and high angles of attack.

Improvements over baseline design were obtained. However, further studies on wing and tail efficiency, affecting stability, is recommended in order to simplify design of a control system. Generally, regarding used analysis methods, Navier-Stokes results confirm integrated overall trends in Euler results, but flow details were naturally influenced by viscosity and they could be quite different.

Acknowledgement

The authors want to thank the Swedish Air Material Defense Agency (FMV) for funding this study under the national research program FoT25 in 2005. Geometry lofting done by Karl-Erik Eklund and Ronny Gyllensten is greatly appreciated as well as discussions held with our Saab colleague Ulf Clareus.

References

[1] Torngren L., *Transonic wind tunnel tests of a swept supercritical wing-body model,PT8.* FFA TN 1982-24, Stockholm 1985.

[2] Eds. Oswatisch K, Rues D. *Symposium Transonicum II.* Springer–Verlag, Berlin Heidelberg New York, 1976.

[3] Cheng H.K., Hafez M.M. Transonic Equivalence Rule: A Nonlinear problem Involving Lift. *Journal of Fluid Mechanics.* Vol 72, Part 1, 1975, pp. 764-766.

[4] Sedin Y. C-J. , Qualitative Calculations of Drag-Rise Characteristics Using the Equivalence Rule. *Proc of the 11th ICAS Congress.* Lisbon, Sept 10-16, 1978.

[5] *Transonic aerodynamics*. Progress in Astronautics and Aeronautics, Vol 81. Editor Nixon, D. Published by AIAA, 1982.

[6] Eliasson, P., 'EDGE', a Navier-Stokes solver for unstructured grids. *Proc to Finite Volumes for Complex Applications III,* ISBN 1 9039 96341, pp. 527-534, 2002.

[7] Woodward, F.A., Analysis and Design of Wing-Body Combinations at Subsonic and Supersonic Speeds. *AIAA J. of Aircraft*, Vol. 5, , pp 528-534, June 1968.

[8] Drela, M., *A users guide to MSES 2.5.* MIT, 1993.

[9] Sedin Y. C-J. ,'PROFAN': An airfoil geometry-analysis and modification program. *Internal Saab report L-01- B567, 1987* (In Swedish, title is translated).

[10] Clareus, U., FoT 25. Concept study URAV/UCAV. Part 4. Main Report: Aero-design. *Internal Saab Report, TDAA-2005-0259.* (Classified. Report in Swedish, title translated).

[11] Wallin, S., Johansson, A.V. An explicit algebraic Reynolds stress model for incompressible and compressible turbulent flows. *Journal of Fluid Mechanics.* 403, 2000, pp 89-132.

[12] Hellsten, A., On the solid-wall boundary condition for w in the k-ω type turbulence modes. *Scientific Report. Report No B-50, Series B.* Helsinki University of Technology, 1998.